

# Data analysis of *ab initio* effective Hamiltonians in iron-based superconductors — Construction of predictors for superconducting critical temperature

Kota Ido<sup>1</sup>, Yuichi Motoyama<sup>1</sup>, Kazuyoshi Yoshimi<sup>1</sup> and Takahiro Misawa<sup>1,2</sup>

<sup>1</sup>*Institute for Solid State Physics, University of Tokyo,  
5-1-5 Kashiwanoha, Kashiwa, Chiba 277-8581, Japan and*

<sup>2</sup>*Beijing Academy of Quantum Information Sciences, Haidian District, Beijing 100193, China*

High-temperature superconductivity occurs in strongly correlated materials such as copper oxides and iron-based superconductors. Numerous experimental and theoretical works have been done to identify the key parameters that induce high-temperature superconductivity. However, the key parameters governing the high-temperature superconductivity remain still unclear, which hamper the prediction of superconducting critical temperatures ( $T_c$ s) of strongly correlated materials. Here by using data-science techniques, we clarified how the microscopic parameters in the *ab initio* effective Hamiltonians correlate with the experimental  $T_c$ s in iron-based superconductors. We showed that a combination of microscopic parameters can characterize the compound-dependence of  $T_c$  using the principal component analysis. We also constructed a linear regression model that reproduces the experimental  $T_c$  from the microscopic parameters. Based on the regression model, we showed a way for increasing  $T_c$  by changing the lattice parameters. The developed methodology opens a new field of materials informatics for strongly correlated electron systems.

## I. INTRODUCTION

The discovery of the high- $T_c$  superconductivity in the copper oxides has inspired a huge amount of studies to clarify the relation between electronic correlations and high- $T_c$  superconductivity[1]. In 2008, the discovery of another high- $T_c$  superconductivity in iron-based superconductors renewed the interest in the superconductivity induced by the electronic correlations[2]. Theoretical and experimental studies of these high- $T_c$  superconductors have revealed that electronic correlations such as Coulomb interactions are key factors that stabilize the high- $T_c$  superconductivity.[3–5] However, it remains unclear how the electronic correlations correlate with  $T_c$ .

Recent theoretical progress enables us to determine the microscopic parameters in the low-energy effective Hamiltonians of solids in an *ab initio* way. The method is often referred to as the *ab initio* downfolding method[6]. Through this method, based on the band structures obtained from the density functional theory (DFT) calculations, screened interactions (e.g., Coulomb interactions) in the low-energy effective Hamiltonians are calculated using the constrained random phase approximation (cRPA) method[7]. By solving the low-energy effective Hamiltonians, we can evaluate the physical properties of strongly correlated materials in a fully *ab initio* way beyond the DFT calculations. It has been shown that the scheme can reproduce the ground-state phase diagrams of the high- $T_c$  superconductors[8, 9].

The combination of an *ab initio* downfolding scheme and an accurate analysis of the derived Hamiltonians is useful for clarifying the mechanism of the high- $T_c$  superconductivity. However, application of this method has been limited to a few compounds due to the high numerical cost associated with the accurate analysis of the effective Hamiltonians. The difficulty of solving the effective Hamiltonians prevents us from gaining a deep un-

derstanding of the high- $T_c$  superconductivity and designing new high- $T_c$  superconductors. Therefore, to predict new superconductors based on the theoretical calculations, development of an alternative and efficient method without solving *ab initio* Hamiltonians is desirable.

Data-driven approaches, such as high-throughput screening, regression analysis, and multivariate statistics, have been used for discovering and designing new compounds with high functionality[10]. Stimulated by the recent progress of data-science, data-driven analyses focused on superconductors have been performed[11–19]. For example, in Ref. [14], utilizing the existing database, the authors constructed regression models for predicting  $T_c$  based on the information of the chemical-composition data of the compounds and the DFT calculations. Their analysis offers several important insights into the relation between the chemical composition and  $T_c$ . However, the effects of electronic correlations in the compounds have not been directly considered in the existing database. Electronic correlations are key factors that stabilize the high- $T_c$  superconductivity and hence the analysis of datasets that explicitly include the information about the electronic correlations is desirable.

From the early stage of studies of the iron-based superconductors, it has been demonstrated that the *ab initio* approach such as the derivation of the band structures and the effective Hamiltonians is useful for clarifying the magnetism [20, 21] and superconductivity [22–24]. In particular, *ab initio* evaluations of the microscopic parameters in the effective Hamiltonians give an insight in understanding the variety of the iron-based superconductors [25]. In this paper, to elucidate the relation between the compound dependence of  $T_c$  and the microscopic parameters, we derive the low-energy effective Hamiltonians for 32 iron-based superconductors and 4 related compounds. These superconductors offer an ideal platform for examining the relation between  $T_c$  and the correlation effects because  $T_c$  and the strength of the correlations

largely depend on the compounds.

Based on the obtained low-energy effective Hamiltonians, rather than directly solving the Hamiltonians, we analyze the relations between the experimentally observed  $T_c$  and the microscopic parameters comprising these Hamiltonians. This analysis is performed using the data-science techniques such as principal component analysis (PCA) and construction of a linear regression model. Through the PCA, we find that the compound dependence is well characterized by the first and second principal components and that the first (second) component consists mainly of the Coulomb interactions (hopping parameters). For example, we find that 1111 compounds have a similar first component and the difference in these compounds is characterized by the second component. We also show that the compound dependence of  $T_c$  with respect to the second principal component is manifested as a dome structure. This result indicates that the microscopic parameters comprising the effective Hamiltonians provide sufficient information for describing the compound dependence.

We also construct a linear regression model, which reproduces the experimentally observed  $T_c$  from the microscopic parameters comprising the effective Hamiltonians. The obtained model succeeds in reproducing the materials dependence of  $T_c$ , as evidenced by a high coefficient of determination ( $R^2 \sim 0.92$ ). We show that our regression model can predict a way to enhance the  $T_c$  of LaFeAsO by changing the structure of the material.

This paper is organized as follows: In Sec. II, we denote the basics of the target materials and explain the *ab initio* downfolding method. In Sec. III A, we show the compound dependence of the microscopic parameters including the electronic correlations in the obtained low-energy effective Hamiltonians. In Sec. III B, we perform PCA aimed at identifying the main parameters that describe the iron-based superconductors using the obtained Hamiltonians. We also construct a regression model that reproduces  $T_c$  from the microscopic parameters. Based on this model, we show a way to optimize  $T_c$  of the iron-based superconductors. A summary and issues that will be addressed in future work are presented in Sec. IV.

## II. METHOD

In this section, we briefly explain the numerical methods we employed, namely the *ab initio* downfolding method, the PCA, and the construction of a linear regression model.

### A. *Ab initio* downfolding method

The DFT calculations of the target materials are performed using QUANTUM ESPRESSO[26]. As the pseudopotential set, we use sg15 library[27], which includes

the optimized norm-conserving Vanderbilt pseudopotentials (ONCVSP)[28]. We replace the pseudopotentials for Gd, Nd, Pr, Ce, and Sm, and Tb with that of La to eliminate the  $f$  metallic bands around the Fermi energy. This approach has been already applied to derivation of *ab initio* parameters for cuprates with a lanthanoid[29]. We use a  $12 \times 12 \times 12$   $k$ -mesh in the first Brillouin zone to perform self-consistent calculations. The optimized tetrahedron method is employed for the DFT calculations[30]. An energy cutoff of 120 (480) Ry is set for plane waves (charge densities).

To derive effective Hamiltonians for our target materials, we use RESPACK [31]. In this work, we construct effective models that are the ten-orbital models consisting of  $3d$  orbitals associated with transition metals (TMs), e.g., Fe, Mn, and Ni. The Hamiltonians are given as follows.

$$H = H_{1\text{body}} + H_{2\text{body}}, \quad (1)$$

$$H_{1\text{body}} = \sum_{i,j} t_{ij,\sigma} c_{i\sigma}^\dagger c_{j\sigma}, \quad (2)$$

$$H_{2\text{body}} = \frac{1}{2} \sum_{i,j,\sigma,\rho} \left( V_{ij} c_{i\sigma}^\dagger c_{j\rho}^\dagger c_{j\rho} c_{i\sigma} + J_{ij} (c_{i\sigma}^\dagger c_{j\rho}^\dagger c_{i\rho} c_{j\sigma} + c_{i\sigma}^\dagger c_{i\rho}^\dagger c_{j\rho} c_{j\sigma}) \right), \quad (3)$$

where  $c_{i\sigma}^\dagger$  ( $c_{i\sigma}$ ) denotes the creation (annihilation) operator of an electron with spin  $\sigma$  at the  $i$ -th maximally localized Wannier function (MLWF)[32, 33]. The indices of the MLWFs include the position of the unit cell  $\mathbf{R}$ , the orbital degrees of freedom  $\mu$  and the index of the TM  $n$ , i.e.,  $i = (\mathbf{R}, \mu, n)$ . Note that the unit cell contains two TMs.  $t_{ij,\sigma}$  in the one-body part of the effective Hamiltonians ( $H_{1\text{body}}$ ) represents the hopping parameters of an electron with spin  $\sigma$  between the  $i$ -th and  $j$ -th MLWFs. When we construct the MLWFs, the  $x$ - $y$  axis is rotated by  $45^\circ$  from the  $a$ - $b$  axis of the unit cell. For this condition, the  $x$ - $y$  axis is parallel to the nearest TM-TM directions. Two-body interactions such as Coulomb interactions ( $V_{ij}$ ) and the exchange interactions ( $J_{ij}$ ) are obtained via cRPA calculations[7]. We set an energy cutoff of 20 Ry for the dielectric function and calculate dielectric functions using more than 100 bands. In both calculations, we use  $6 \times 6 \times 6$   $k$  points for the 122 systems and  $8 \times 8 \times 4$   $k$  points for the others.

The *ab initio* downfolding method based on cRPA has been applied to a wide range of the correlated electron systems including iron-based superconductors [25, 34] and cuprates [29, 35, 36]. Through these applications, it is shown that the downfolding method gives realistic values of the Coulomb and exchange interactions. However, there are several variations of the cRPA method such as the treatment of the band disentangle [33, 37, 38]. The quantitative results may depend on the details of the methods. For example, in the derivation of the single-band Hubbard-type Hamiltonians of the cuprates, it is pointed out [36] that the values of onsite Coulomb interactions depend on the downfolding methods [29, 35, 36].

We expect that this subtle problem does not exist in the derivation of the ten-orbital Hamiltonians in the iron-based superconductors since the ten bands cover almost all the degrees of freedom near the Fermi energy. Therefore, we use the cRPA method with the conventional band-disentanglement treatment [33] implemented in RESPACK to capture the overall trend of the compound dependence of the effective Hamiltonians.

For the 122 family, an *ab initio* model including  $d$  orbitals of alkaline earth metals such as Ba is more appropriate (than other models) because these bands are located above but near the Fermi level[39]. Nevertheless, using 10  $d$  orbitals in TM atoms, we can construct the MLWFs that reproduce the DFT band structure below the energy associated with the  $d$  band of alkaline earth metals.

Using the derived microscopic parameters, we employ the following typical parameters as descriptors for the data analysis,

$$t_{p,q} = g_p (|t_{(0,\mu,0),(0,\nu,1)}| \cdot \Delta_q(\mu, \nu)), \quad (4)$$

$$t'_{p,q} = g_p (|t_{(0,\mu,0),(\mathbf{R}_a,\nu,0)}| \cdot \Delta_q(\mu, \nu)), \quad (5)$$

$$U_{p,q} = g_p (V_{(0,\mu,0),(0,\nu,0)} \cdot \Delta_q(\mu, \nu)), \quad (6)$$

$$V_{p,q} = g_p (V_{(0,\mu,0),(0,\nu,1)} \cdot \Delta_q(\mu, \nu)), \quad (7)$$

$$V'_{p,q} = g_p (V_{(0,\mu,0),(\mathbf{R}_a,\nu,0)} \cdot \Delta_q(\mu, \nu)), \quad (8)$$

$$J_{p,q} = g_p (J_{(0,\mu,0),(0,\nu,1)} \cdot \Delta_q(\mu, \nu)), \quad (9)$$

where  $\mathbf{R}_a$  is a primitive translation vector along the  $a$  axis.  $\Delta_q(\mu, \nu)$  specifies orbital information;  $\Delta_{\text{all}}(\mu, \nu) = 1$ ,  $\Delta_{\text{diag}}(\mu, \nu) = \delta_{\mu,\nu}$ , and  $\Delta_{\text{offdiag}}(\mu, \nu) = 1 - \delta_{\mu,\nu}$ .  $g_p$  is a function for extracting a feature of the derived microscopic parameters among all combinations of  $\mu$  and  $\nu$ . We use three types of  $g_p$ : a function that returns the maximum value (p=max), a function that returns the mean value (p=mean), and a function that returns the minimum value (p=min). We exclude  $t_{\min}$  and  $t'_{\min}$  because these are zero. Throughout this paper,  $t_{\max} = t_{\max, \text{all}}$ ,  $\bar{U} = U_{\text{mean, diag}}$ ,  $\bar{V} = V_{\text{mean, diag}}$ , and  $\bar{J} = J_{\text{mean, offdiag}}$  for simplicity.

## B. PCA

It is expected that the difference in the parameters of the derived effective Hamiltonians can characterize various target materials. To verify this hypothesis, we visualize the relationship between the parameters and extract the main parameters that govern the materials dependence via PCA. The PCA, which has been applied to a dataset obtained for superconductors [40], leads to a reduction in the dimensionality of a dataset, thereby providing information on the principal components of the target dataset. We note that the results of PCA depend on the employed data set. In this study, we perform PCA analysis for the Hamiltonians of the compounds with high  $T_c$  to clarify the microscopic parameter dependence of  $T_c$ .

Here, we briefly explain basics of the PCA [41]. Using the descriptor vector  $\mathbf{x}^{(n)}$  of the  $n$ -th data (where  $n$  corresponds to the index of materials), we construct the covariance matrix  $C$ , which is defined as

$$C_{ij} = \frac{1}{N-1} \sum_n x_i^{(n)} x_j^{(n)}, \quad (10)$$

where  $N$  is the total number of the materials. We note that the average value of the descriptors over the materials is set to 0 ( $\sum_n x_i^{(n)} = 0$ ) and its standard deviation  $\sqrt{\sum_n (x_i^{(n)})^2 / N}$  is set to 1. By diagonalizing  $C$ , we obtain the principal vectors  $\mathbf{v}^m$  with the principal values  $\lambda_m$  ( $\lambda_m$ 's are sorted in descending order). The first principal vector  $\mathbf{v}^1$  represents the direction associated with the most diverse data. Using the principal vectors  $\mathbf{v}^m$ , we can project the descriptor vectors onto the principal vectors and obtain the  $m$ th principal value  $y_m^{(n)}$  as follows,

$$y_m^{(n)} = \sum_i x_i^{(n)} v_i^m. \quad (11)$$

In Sec. IIIB, we show that the materials dependence can be characterized by the principal values.

## C. Construction of regression model

We construct a linear regression model  $f$  for reproducing  $T_c$  from the parameters of the effective Hamiltonian,

$$f(\mathbf{x}; \mathbf{w}) = w_0 + \sum_{i=1}^{N_f} x_i w_i. \quad (12)$$

To introduce non-linearity, we inserted the quadratic terms and the ratio terms (such as  $t_{\max} \bar{U}$  and  $\bar{V}/U_{\max}$ ) between the original parameters. (please see Appendix A for further details of the descriptors).

The number of samples in our dataset is comparable to that of the descriptors, and hence we should carefully control the number of the descriptors in the regression models to avoid overfitting. Therefore, we prepared models where some descriptors were dropped in a systematic way — for example, one model has only hopping parameters as descriptors, another one has hopping and onsite-Coulomb interactions, and yet another one has hopping, onsite-Coulomb and the cross term between these parameters (for details, see Appendix A). To identify the optimal model among these models, we calculate the *scores* associated with each model. One of the simplest ways to estimate score is the hold-out validation (HV) method [Fig. 1 (a)]. For this method, we first split the original dataset (white boxes in Fig. 1) into two parts, the training dataset (blue boxes) and the validation dataset (red boxes). The model is optimized by using the training

dataset and a training algorithm with the hyperparameter  $\alpha^{(m)}$ . The score of the model  $m$  is calculated as follows,

$$S_{\text{HV}}^{(m)} = \sum_{n \in D_{\text{validation}}} \frac{\left[ T_c^{(n)} - f(\mathbf{x}^{(n)}; \mathbf{w}^{(m)}) \right]^2}{N_{\text{validation}}}, \quad (13)$$

where  $D_{\text{validation}}$  is the validation dataset,  $T_c^{(n)}$  is the experimental  $T_c$  of the material labeled with  $n$  and  $N_{\text{validation}}$  is the number of the validation data. The model with a minimum score is chosen as the optimal model.

While the HV method has a bias from how to split the dataset, the cross-validation (CV) method reduces it. In this study, we employ the nested CV method [42], whose procedure is shown in Fig. 1 (b). In the following, we explain the procedure of the nested CV method.

(i) **Outer CV:** We first split the original dataset by the leave-one-out CV (LOOCV) method, which corresponds to the outer CV. In the outer CV, each model ( $m$ ) is trained by an algorithm with its hyperparameter  $\alpha^{(m)}$ .

(ii) **Inner CV:** To tune  $\alpha^{(m)}$  for  $k$ -th split dataset as  $\alpha_k^{(m)}$ , we again apply the LOOCV method to the training data with  $N - 1$  samples of  $k$ -th training dataset, which is called the inner CV.

(iii) **Determination of  $\alpha$ :** In this inner CV process, we optimize the weights of the model  $\mathbf{w}_{kl}^{(m)}$  by minimizing LASSO (least absolute shrinkage and selection operator)[43] type cost function;

$$L(\mathbf{w}_{kl}^{(m)}; \alpha_k^{(m)}) = \sum_{n \in D_{\text{training}}^{kl}} \frac{\left[ T_c^{(n)} - f(\mathbf{x}^{(n)}; \mathbf{w}_{kl}^{(m)}) \right]^2}{N_{\text{training}}^{kl}} + \alpha_k^{(m)} |\mathbf{w}_{kl}^{(m)}|, \quad (14)$$

where  $D_{\text{training}}^{kl}$  is the  $l$ -th training dataset in the inner CV and  $N_{\text{training}}^{kl}$  is the number of data in  $D_{\text{training}}^{kl}$ , and the coefficient of the  $L_1$  term,  $\alpha_k^{(m)}$  is a hyper parameter of LASSO, which will be tuned by the inner CV. By using obtained  $\mathbf{w}_{kl}^{(m)}(\alpha_k^{(m)})$ , the score for the model  $m$  and  $l$ -th dataset split from  $k$ -th dataset in the outer CV,  $\sigma_{kl}^{(m)}(\alpha_k^{(m)})$  is calculated as

$$\sigma_{kl}^{(m)}(\alpha_k^{(m)}) = \sum_{n \in D_{\text{validation}}^{kl}} \frac{\left[ T_c^{(n)} - f(\mathbf{x}^{(n)}; \mathbf{w}_{kl}^{(m)}(\alpha_k^{(m)})) \right]^2}{N_{\text{validation}}^{kl}}. \quad (15)$$

After scores  $\sigma_{kl}^{(m)}(\alpha_k^{(m)})$  for all inner CV dataset are obtained, the total score of  $\alpha_k^{(m)}$

$$\sigma_{\text{CV},k}^{(m)}(\alpha_k^{(m)}) = \frac{1}{N-1} \sum_{l=1}^{N-1} \sigma_{kl}^{(m)}(\alpha_k^{(m)}) \quad (16)$$

is calculated. Finally, the hyperparameter  $\alpha_k^{(m)}$  is tuned to minimize  $\sigma_{\text{CV},k}^{(m)}(\alpha_k^{(m)})$ . Note that the  $k$ -th dataset

split by the outer CV is split further into  $N - 2$  samples for training ( $N_{\text{training}}^l = N - 2$ ) and one sample for validation ( $N_{\text{validation}}^l = 1$ ) in the inner CV. We use scikit-learn [44] package to solve the LASSO and use Optuna [45] to optimize  $\alpha_k^{(m)}$  by means of the Bayesian optimization method.

(iv) **Evaluation of score:** After  $\alpha_k^{(m)}$  is optimized, the weight of the model  $m$ ,  $\mathbf{w}_k^{(m)}$  in following equation is again optimized by LASSO with  $\alpha_k^{(m)}$  as in the normal CV method, and then the validation score  $S_k^{(m)}$  defined in Eq. (17) is evaluated as follows:

$$S_k^{(m)} = \sum_{n \in D_{\text{validation}}^k} \frac{\left[ T_c^{(n)} - f(\mathbf{x}^{(n)}; \mathbf{w}_k^{(m)}) \right]^2}{N_{\text{validation}}}, \quad (17)$$

where  $D_{\text{validation}}^k$  is the  $k$ -th validation dataset split by the outer CV and  $N_{\text{validation}} = 1$ .

(v) **Average of score:** The final score  $S_{\text{CV}}^{(m)}$  is then calculated from the following equation.

$$S_{\text{CV}}^{(m)} = \frac{1}{N} \sum_{k=1}^N S_k^{(m)}. \quad (18)$$

(vi) **Determination of the best model:** By performing the nested CV for all the models we define, we obtain the best model  $m^*$  with the lowest score, i.e.  $m^* = \text{argmin}_m S_{\text{CV}}^{(m)}$ .

### III. RESULTS

#### A. *Ab initio* results

We obtain the low-energy effective Hamiltonians for the 11-family (e.g., FeSe), 1111-family (e.g., LaFeAsO), 111-family (e.g., LiFeAs), 122-family (e.g., BaFe<sub>2</sub>As<sub>2</sub>), and 42622-family (e.g., Ca<sub>4</sub>Al<sub>2</sub>O<sub>6</sub>Fe<sub>2</sub>As<sub>2</sub>). For comparison with the iron-based superconductors, we have also obtained the low-energy effective Hamiltonians for Mn (e.g., BaMnAsF) and Ni (e.g., LaNiAsO) analogs of the iron-based superconductors. Each target material is categorized as one of the above-mentioned families based on the chemical composition of the materials.

The typical microscopic parameters (such as the maximum values of the hopping parameters and the averaged onsite-Coulomb interactions) comprising the low-energy effective Hamiltonians and the families of our target compounds are listed in Table I. The numerical conditions of the *ab initio* calculations are detailed in Sec. II A. The crystal structures of all the target materials except for Ca<sub>4</sub>Al<sub>2</sub>O<sub>6</sub>Fe<sub>2</sub>P<sub>2</sub>, GdFePO and NdFePO are obtained from the experiments. Most of them are obtained from the Inorganic Crystal Structure Database (ICSD)[46, 47] and SpringerMaterials[48]. We note that we employ a tetragonal crystal phase at ambient pressure. For calculations of Ca<sub>4</sub>Al<sub>2</sub>O<sub>6</sub>Fe<sub>2</sub>P<sub>2</sub> (GdFePO and NdFePO), the

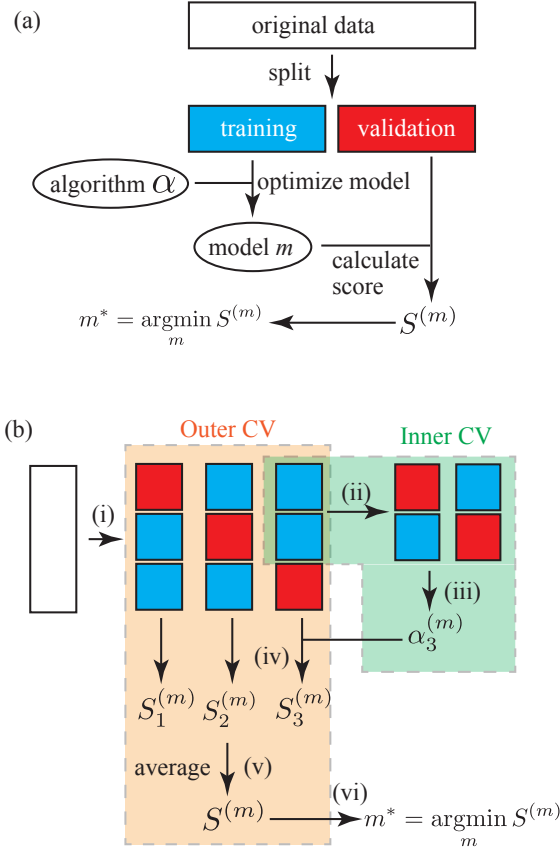


FIG. 1. (color online) Schematic picture of the validation methods. (a) Hold-out validation, which is a basic method for validating. In this method, we split the original data (white rectangle) into the training data (blue) and the validation data (red). Each model  $m$  is optimized by the training dataset and the training algorithm with the hyperparameter  $\alpha^{(m)}$ . Once the model is optimized, the score of the model  $S^{(m)}$  is calculated by using the validation data. (b) Nested CV, which is the method used in the present study. Details of each step (i)-(vi) are explained in main text.

fractional coordinates of the atoms are used as the same as those of  $\text{Ca}_4\text{Al}_2\text{O}_6\text{Fe}_2\text{As}_2(\text{PrFePO})$ , and the lattice constant is employed from the experiment.

We find that the amplitudes of the hopping parameters and the Coulomb interactions exhibit a strong dependence on the compounds. For example,  $\bar{U}/t_{\text{max}}$  of  $\text{FeSe}$  ( $\bar{U}/t_{\text{max}} = 10.11$ ) is approximately twice that of  $\text{GdFePO}$  ( $\bar{U}/t_{\text{max}} = 5.15$ ). This significant variation indicates that iron-based superconductors offer an ideal platform for examining the relation between  $T_c$  and the microscopic parameters. We note that the overall tendency of the obtained parameters is consistent with the tendency revealed by previous calculations [25, 49]. In particular, the averaged Coulomb interaction  $\bar{U}$  values agree (to within

10%) with those obtained in the previous studies, except for  $\text{BaFe}_2\text{As}_2$ . The  $\bar{U}$  value of  $\text{BaFe}_2\text{As}_2$  is  $\sim 20\%$  smaller than that reported in the previous study [25]. This deviation may have resulted from the difference between the disentangle treatment for the Ba  $d$  band near the Fermi level. We neglect clarification of this difference because (in the present study) we focus on the relation between the  $T_c$  and overall compound dependence of the microscopic parameters.

In Fig. 2 (a-d), we plot the compound dependence of the typical microscopic parameters. We find that the effective onsite interaction  $\bar{U}/t_{\text{max}}$  value of the target materials varies significantly (from five to ten). A significant variation was also noted in Ref. [25] where six iron based superconductors were analyzed. The Hund coupling  $\bar{J}$  is also dependent on the materials, although its range is narrower than that of  $\bar{U}$ .

From the results obtained for the 1111 family, the compounds can be classified into three categories, namely 1111 compounds with P (1111-P), with As (1111-As), and with F or H (1111-F,H). We find that stronger effective Coulomb interactions  $\bar{U}/t_{\text{max}}$  occur in 1111-F,H than in the other 1111 compounds, owing to the larger  $\bar{U}$  compared with those of 1111-P and 1111-As. However, the difference between the  $\bar{U}/t_{\text{max}}$  values of 1111-P and 1111-As stems from transfer integrals associated with the difference in the localization of MLWF, as noted in Ref. [25]. A similar tendency is observed for the 111 family.

The *ab initio* parameters of the relevant compounds are similar to those of iron-based superconductors. Mn compounds have strong effective interactions  $\bar{U}/t_{\text{max}}$ , which arise from the smaller hopping integrals than those of other compounds. We note that their occupation numbers in one TM atom are different from those of iron-based superconductors.

Before performing the data-science analyses such as PCA, we examine the influence of the lattice structure on the materials dependence of the microscopic parameters. The importance of the anion [chalcogen (Ch) or pnictide (Pn)] position is pointed out in the previous studies [78, 79], and hence we plot the typical microscopic parameters as a function of the distance between Ch/Pn and TM [see Fig. 2(e-h)]. As shown in Fig. 2 (e), the magnitude of the effective onsite Coulomb interaction  $\bar{U}/t_{\text{max}}$  increases with increasing distance. As shown in Fig. 2 (f) and (g), we find that this trend is mainly governed by  $t_{\text{max}}$ , i.e.,  $t_{\text{max}}$  decreases almost monotonically with increasing the distance whereas  $\bar{U}$  is almost independent of the distance. This result indicates that the difference between the distances controls  $t_{\text{max}}$  mainly through the hybridization between TM  $d$  orbitals and Ch/Pn  $p$  orbitals. We note that  $\bar{J}$  exhibits no clear distance dependence.

TABLE I. Compound-dependence of *ab initio* parameters for target materials.  $t_{\max}$  denotes the maximum value of the hopping parameters between the nearest-neighbor transition metals (TMs).  $\bar{U}$  and  $\bar{J}$  denote the averaged values of the diagonal onsite Coulomb interactions and the onsite Hund coupling over the TM  $d$  orbitals, respectively.  $\bar{V}$  is the averaged value of the diagonal density-density interactions between the nearest-neighbor TM sites. The unit of the interaction and hopping parameters is given in eV. The effective interactions  $\bar{U}/t_{\max}$ ,  $\bar{V}/t_{\max}$ , and  $\bar{J}/t_{\max}$  are also listed. Ref shows the reference of the crystal structures we employed. Information about the microscopic parameters will be public elsewhere.

material	family	$t_{\max}$ (eV)	$\bar{U}$ (eV)	$\bar{V}$ (eV)	$\bar{J}$ (eV)	$\bar{U}/t_{\max}$	$\bar{V}/t_{\max}$	$\bar{J}/t_{\max}$	Ref
FeS	11	0.46	4.53	1.20	0.55	9.91	2.63	1.21	[50]
FeSe	11	0.41	4.14	1.04	0.55	10.11	2.53	1.33	[51]
FeTe	11	0.37	3.15	0.73	0.50	8.57	1.98	1.37	[52]
CaFeAsH	1111	0.37	2.71	0.70	0.44	7.26	1.88	1.19	[53]
SrFeAsF	1111	0.37	3.13	0.88	0.47	8.44	2.38	1.26	[54]
CaFeAsF	1111	0.38	3.01	0.87	0.46	7.96	2.30	1.21	[55]
LaFePO	1111	0.43	2.40	0.65	0.40	5.59	1.51	0.92	[56]
PrFePO	1111	0.43	2.44	0.65	0.40	5.62	1.51	0.93	[57]
NdFePO	1111	0.44	2.44	0.66	0.40	5.51	1.49	0.90	[57]
SmFePO	1111	0.45	2.44	0.66	0.40	5.45	1.47	0.89	[57]
GdFePO	1111	0.47	2.40	0.66	0.39	5.15	1.41	0.84	[57]
LaFeAsO	1111	0.36	2.46	0.61	0.43	6.90	1.72	1.19	[2]
CeFeAsO	1111	0.36	2.49	0.62	0.43	6.88	1.72	1.18	[58]
PrFeAsO	1111	0.36	2.50	0.62	0.43	6.91	1.72	1.19	[59]
NdFeAsO	1111	0.36	2.51	0.62	0.44	6.95	1.71	1.22	[59]
SmFeAsO	1111	0.37	2.51	0.63	0.43	6.84	1.71	1.17	[59]
GdFeAsO	1111	0.37	2.52	0.63	0.44	6.73	1.67	1.16	[60]
TbFeAsO	1111	0.37	2.52	0.63	0.43	6.76	1.69	1.15	[59]
LiFeP	111	0.50	3.09	0.90	0.45	6.23	1.82	0.90	[61]
LiFeAs	111	0.42	3.02	0.78	0.47	7.17	1.86	1.12	[62]
NaFeAs	111	0.39	3.06	0.79	0.48	7.86	2.02	1.23	[63]
KFe <sub>2</sub> P <sub>2</sub>	122	0.34	2.43	0.61	0.45	7.20	1.81	1.32	[64, 65]
SrFe <sub>2</sub> P <sub>2</sub>	122	0.46	2.72	0.74	0.43	5.86	1.59	0.93	[66]
CaFe <sub>2</sub> P <sub>2</sub>	122	0.42	2.81	0.60	0.52	6.75	1.44	1.24	[67]
BaFe <sub>2</sub> P <sub>2</sub>	122	0.45	2.51	0.64	0.43	5.56	1.42	0.95	[68]
KFe <sub>2</sub> As <sub>2</sub>	122	0.47	3.07	0.94	0.46	6.59	2.03	0.98	[69]
SrFe <sub>2</sub> As <sub>2</sub>	122	0.37	2.62	0.64	0.44	7.09	1.74	1.20	[67]
CaFe <sub>2</sub> As <sub>2</sub>	122	0.37	2.38	0.52	0.44	6.36	1.39	1.18	[70]
BaFe <sub>2</sub> As <sub>2</sub>	122	0.36	2.40	0.55	0.45	6.59	1.50	1.22	[71]
Sr <sub>4</sub> Sc <sub>2</sub> O <sub>6</sub> Fe <sub>2</sub> P <sub>2</sub>	42622	0.41	2.99	0.86	0.45	7.31	2.11	1.09	[72]
Ca <sub>4</sub> Al <sub>2</sub> O <sub>6</sub> Fe <sub>2</sub> P <sub>2</sub>	42622	0.42	3.00	0.93	0.45	7.10	2.21	1.07	[73]
Ca <sub>4</sub> Al <sub>2</sub> O <sub>6</sub> Fe <sub>2</sub> As <sub>2</sub>	42622	0.41	2.95	0.90	0.45	7.12	2.16	1.09	[73]
BaMnAsF	Mn	0.29	2.75	0.77	0.45	9.43	2.64	1.55	[74]
BaMn <sub>2</sub> As <sub>2</sub>	Mn	0.31	2.33	0.57	0.43	7.47	1.82	1.36	[75]
BaNi <sub>2</sub> As <sub>2</sub>	Ni	0.42	2.81	0.48	0.47	6.64	1.15	1.11	[76]
LaNiAsO	Ni	0.39	2.81	0.61	0.44	7.11	1.55	1.11	[77]

## B. Data analysis

By using the effective Hamiltonians reported in the previous section, we perform the PCA and the regression analysis for  $T_c$  of iron-based superconductors. We focus on the superconductivity of the iron-based superconductors in this study, since the  $T_c$  values of Ni compounds

are very low, and Mn compounds exhibit no superconductivity. The results obtained from our data analysis are summarized in Table II. We provide details of the PCA analysis and the construction of the regression model in subsequent sections.

Here, we detail our strategy for assigning  $T_c$  to the effective Hamiltonians. Since the superconductivity ap-

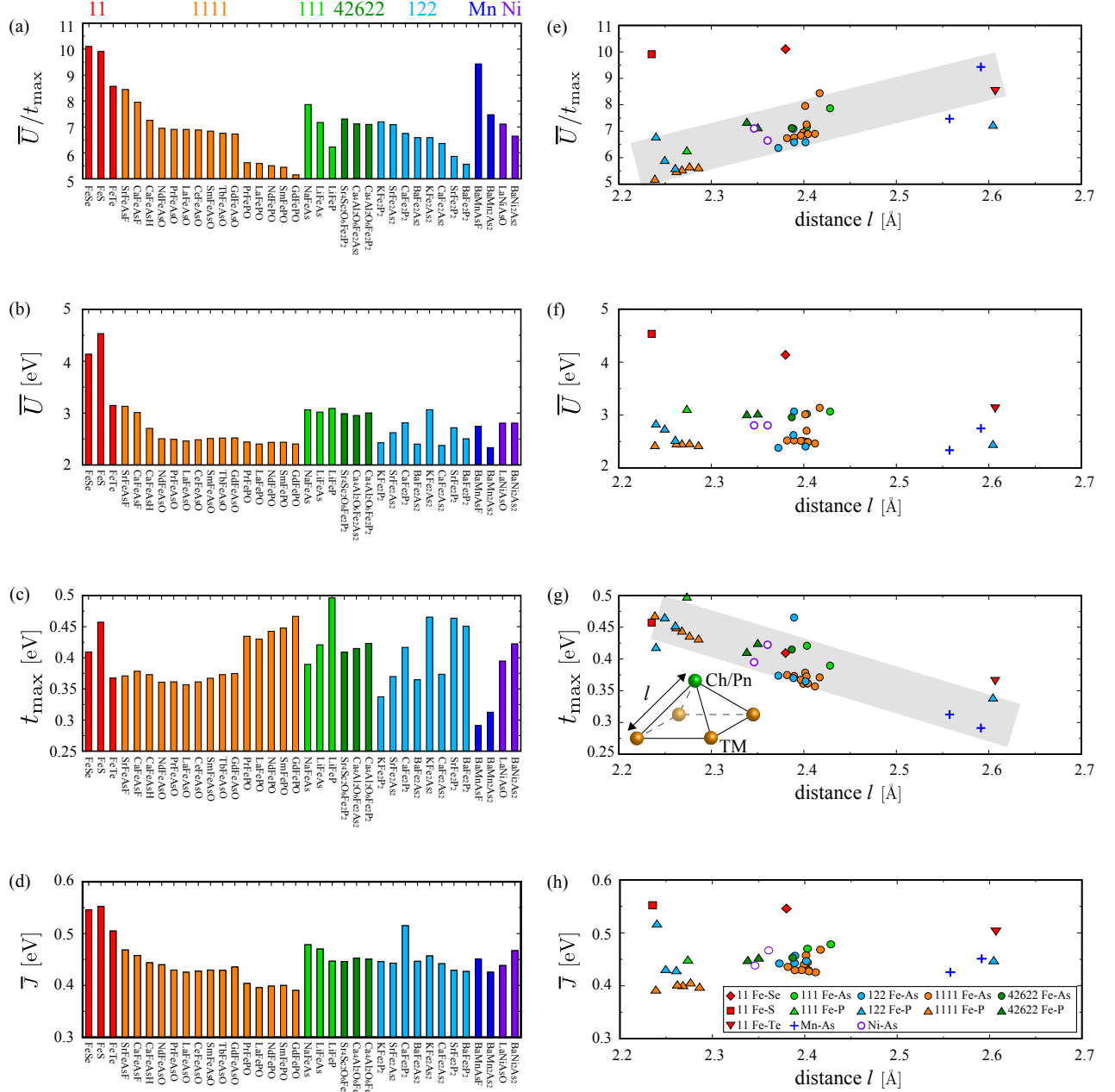


FIG. 2. (color online) *Ab initio* parameters for iron-based superconductors and the related compounds. These definitions are explained in the caption of Table I. (a-d) Compound-dependence of *ab initio* parameters for (a)  $\bar{U}/t_{\max}$ , (b)  $\bar{U}$ , (c)  $t_{\max}$ , and (d)  $\bar{J}$ . Colors represent the family name: red bars are the results for the 11 family, orange bars are the results for the 1111 family, light-green bars are the results for the 111 family, green bars are the results for the 42622 family, light-blue bars are the results for the 122 family, blue bars are the results for the Mn compounds, and purple bars are the results for the Ni compounds. (e-h) *Ab initio* parameters as a function of the distance of TM from Ch/Pn. Legends denote the kinds of TM and Ch/Pn of the target materials. Filled, open and cross symbols represent the results of Fe, Ni and Mn compounds, respectively. For the classification of the family name, the same colors of the symbols are employed as those in the panels (a-d).  $l$  is the distance between TM and Ch/Pn, which is schematically shown in the inset in panel (g). Gray thick lines in panels (e) and (g) are guides for the eye.

pears in the doped compounds, it is the best way to derive the low-energy effective Hamiltonians for the doped

compounds. When we can obtain the information of the lattice structures for both end compounds (e.g. FeSe and

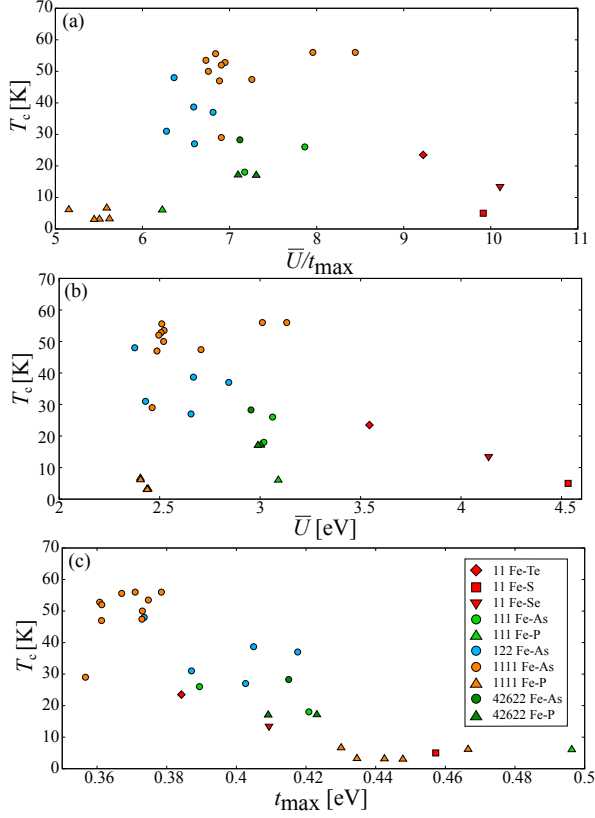


FIG. 3. (color online) Plot of  $T_c$  as a function of (a)  $t_{\max}$ , (b)  $\bar{U}$ , and (c)  $\bar{U}/t_{\max}$ .

FeTe), we interpolate the microscopic parameters of the effective Hamiltonians for the end compounds as shown in Table II. However, information of the lattice structures for the end compounds is not available in most cases for 1111 compounds. Nevertheless, in terms of the microscopic parameters, we can expect the difference is small in the low-doping regime where  $T_c^{\text{exp}}$  shown in Table II was observed. Therefore, we simply assume that the effective Hamiltonian of the closest stoichiometry compound can govern the superconductivity in the doped compounds. As we will show, the PCA analysis shows that the combination of the microscopic parameters well describe the compounds dependence of  $T_c$ . This result supports the validity of the assumption. We also note that the same assumption was used in the analysis of the relation between  $T_c$  and the onsite Coulomb interactions in cuprates [29, 36].

### 1. PCA

Before showing the results of PCA, we first examine how  $T_c$  depends on the typical microscopic parameters such as  $\bar{U}/t_{\max}$ ,  $\bar{U}$ , and  $t_{\max}$ . As shown in Fig.3, We do not find any significant correlation between  $T_c$  and  $\bar{U}$ .

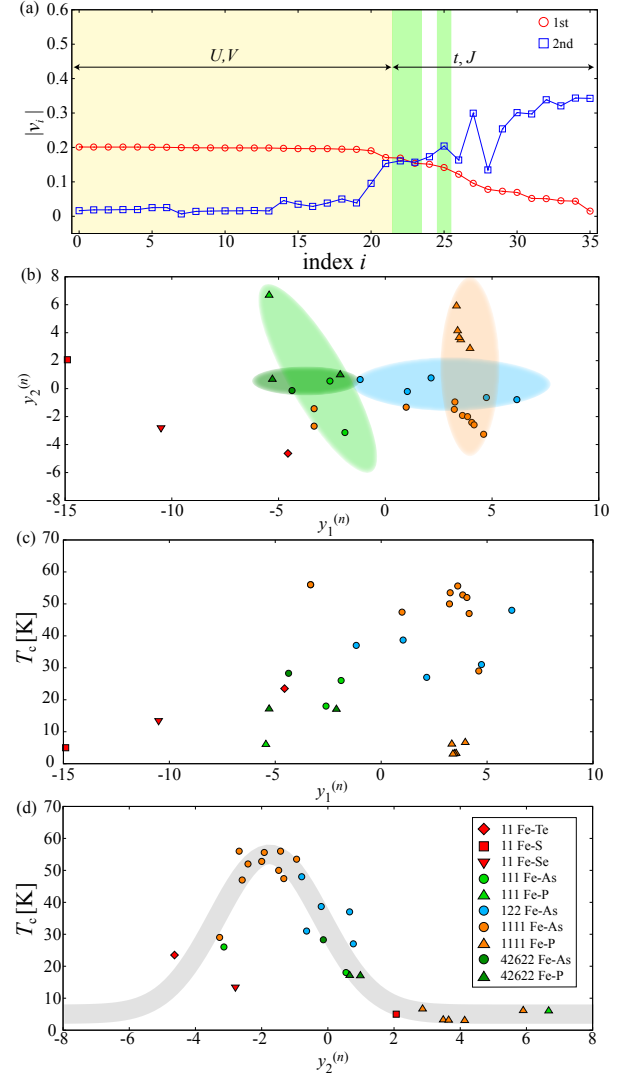


FIG. 4. (color online) PCA analysis of the *ab initio* parameters associated with the iron-based superconductors. (a) Each component of the 1st and the 2nd principal vector. The descriptors are sorted in descending order of the absolute value corresponding to the components of the first principal vector,  $|v_i^1|$ . The interaction parameters (onsite and offsite Coulomb interactions) govern the 1st principal vector, while the hopping parameters and Hund couplings govern the 2nd principal vector. The descriptors in the yellow, green, and white regions are related to the Coulomb interactions, the Hund coupling, and the transfer parameters, respectively. See Appendix A for the features of the descriptors for the PCA and the details of the index  $i$ . (b) Compound-dependence of the 1st and the 2nd principal components, which are defined in Eq. (11). Notations are the same as in panels (c) and (d). Colored ellipses are guides for the eye. (c) and (d)  $T_c$  as functions of the 1st and the 2nd principal component. Gray thick curves are guides for the eye.

On the other hand, we find that  $T_c$  shows a subtle peak structure as a function  $\bar{U}/t_{\max}$  and  $t_{\max}$ . This is in sharp



TABLE II. Superconducting transition temperature  $T_c$  values of target materials. *Ab initio* effective Hamiltonians are used as descriptors for the construction of the regression model.  $T_c^{\text{exp.}}$  and  $T_c^{\text{pred.}}$  denote onset  $T_c$  observed in experiments and  $T_c$  predicted by our regression model, respectively.  $y_1$  and  $y_2$  are the values of the 1st and the 2nd principal components in the PCA, respectively.  $(H_A, H_B)$  denotes the linear interpolation of the parameters between  $H_A$  and  $H_B$ , whose ratio corresponds to the stoichiometric ratio of a target material. The dataset contains 29 materials.

material	family	$T_c^{\text{exp.}}$ (K)	$T_c^{\text{pred.}}$ (K)	$y_1$	$y_2$	Hamiltonian
FeS	11	5 [50]	6.2	-14.89	2.07	$H_{\text{FeS}}$
FeSe	11	13.5 [80]	13.4	-10.51	-2.79	$H_{\text{FeSe}}$
FeSe <sub>0.4</sub> Te <sub>0.6</sub>	11	23.5 [81, 82]	24.3	-4.56	-4.63	$(H_{\text{FeSe}}, H_{\text{FeTe}})$
Ca <sub>0.77</sub> La <sub>0.23</sub> FeAsH	1111	47.4 [83]	55.1	0.98	-1.33	$H_{\text{CaFeAsH}}$
Sr <sub>0.5</sub> Sm <sub>0.5</sub> FeAsF	1111	56 [84]	51.1	-3.33	-2.68	$H_{\text{SrFeAsF}}$
Ca <sub>0.4</sub> Pr <sub>0.6</sub> FeAsF	1111	56 [85]	53.6	-3.33	-1.43	$H_{\text{CaFeAsF}}$
LaFePO	1111	6.6 [86]	3.2	3.97	2.86	$H_{\text{LaFePO}}$
PrFePO	1111	3.2 [86]	8.2	3.54	3.49	$H_{\text{PrFePO}}$
NdFePO	1111	3.1 [86]	4.6	3.46	3.65	$H_{\text{NdFePO}}$
SmFePO	1111	3 [87]	6.4	3.39	4.13	$H_{\text{SmFePO}}$
GdFePO	1111	6.1 [88]	2.5	3.33	5.90	$H_{\text{GdFePO}}$
LaFeAsO <sub>0.92</sub> H <sub>0.08</sub>	1111	29 [89, 90]	43.3	4.60	-3.27	$H_{\text{LaFeAsO}}$
CeFeAsO <sub>0.75</sub> H <sub>0.25</sub>	1111	47 [91]	46.1	4.15	-2.59	$H_{\text{CeFeAsO}}$
PrFeAsO <sub>0.89</sub> F <sub>0.11</sub>	1111	52 [92]	48.4	4.05	-2.41	$H_{\text{PrFeAsO}}$
NdFeAsO <sub>0.8</sub> F <sub>0.2</sub>	1111	52.8 [93]	55.2	3.85	-2.00	$H_{\text{NdFeAsO}}$
SmFeAsO <sub>0.917</sub> F <sub>0.083</sub>	1111	55.6 [94]	48.1	3.61	-1.92	$H_{\text{SmFeAsO}}$
GdFeAsO <sub>0.85</sub>	1111	53.5 [95]	49.5	3.26	-0.95	$H_{\text{GdFeAsO}}$
TbFeAsO <sub>0.9</sub> F <sub>0.1</sub>	1111	50 [96]	46.9	3.23	-1.49	$H_{\text{TbFeAsO}}$
LiFeP	111	6 [61]	5.7	-5.44	6.67	$H_{\text{LiFeP}}$
NaFeAs	111	26 [97]	24.1	-1.89	-3.14	$H_{\text{NaFeAs}}$
Li <sub>0.6</sub> FeAs	111	18 [98]	28.1	-2.60	0.55	$H_{\text{LiFeAs}}$
SrFe <sub>2</sub> As <sub>1.3</sub> P <sub>0.7</sub>	122	27 [99]	31.0	2.15	0.77	$(H_{\text{SrFe}_2\text{As}_2}, H_{\text{SrFe}_2\text{P}_2})$
BaFe <sub>2</sub> As <sub>1.48</sub> P <sub>0.52</sub>	122	31 [100]	33.0	4.73	-0.64	$(H_{\text{BaFe}_2\text{As}_2}, H_{\text{BaFe}_2\text{P}_2})$
K <sub>0.5</sub> Sr <sub>0.5</sub> Fe <sub>2</sub> As <sub>2</sub>	122	37 [101]	26.1	-1.17	0.65	$(H_{\text{KFe}_2\text{As}_2}, H_{\text{SrFe}_2\text{As}_2})$
Ca <sub>0.83</sub> La <sub>0.17</sub> Fe <sub>2</sub> As <sub>1.88</sub> P <sub>0.12</sub>	122	48 [102, 103]	49.0	6.17	-0.79	$H_{\text{CaFe}_2\text{As}_2}$
Ba <sub>0.6</sub> K <sub>0.4</sub> Fe <sub>2</sub> As <sub>2</sub>	122	38.7 [104]	29.2	1.03	-0.20	$(H_{\text{BaFe}_2\text{As}_2}, H_{\text{KFe}_2\text{As}_2})$
Ca <sub>4</sub> Al <sub>2</sub> O <sub>5.80</sub> Fe <sub>2</sub> P <sub>2</sub>	42622	17.1 [73]	19.2	-5.29	0.66	$H_{\text{Ca}_4\text{Al}_2\text{O}_6\text{Fe}_2\text{P}_2}$
Sr <sub>4</sub> Sc <sub>2</sub> O <sub>6</sub> Fe <sub>2</sub> P <sub>2</sub>	42622	17 [72]	18.8	-2.11	0.98	$H_{\text{Sr}_4\text{Sc}_2\text{O}_6\text{Fe}_2\text{P}_2}$
Ca <sub>4</sub> Al <sub>2</sub> O <sub>5.65</sub> Fe <sub>2</sub> As <sub>2</sub>	42622	28.3 [73]	26.9	-4.37	-0.13	$H_{\text{Ca}_4\text{Al}_2\text{O}_6\text{Fe}_2\text{As}_2}$

contrast with the cuprates where it is proposed that  $T_c$  has some correlations with both  $U$  and  $U/t$  [29, 36]. As we show later, from the PCA analysis, we show that  $T_c$  shows a clear peak structure as a function of the second principal component, which mainly consists of the hopping parameters. Thus, although this  $t_{\text{max}}$  dependence roughly captures some aspects of the compound dependence of  $T_c$ , the PCA analysis is a more systematic way for extracting the important descriptors for characterizing the target systems without any prior knowledge.

Here, we explain why the parameter dependence of  $T_c$  is different between iron-based superconductors and cuprates. In iron-based superconductors, the hopping parameters, such as  $t_{\text{max}}$ , mainly change while the Coulomb interactions, such as  $U$ , mainly change in cuprates [29,

36, 105, 106]. This difference can be understood as follows: In iron-based superconductors, the distance between anions and irons (e.g., As and Fe) widely varies, as shown in Fig. 2. This indicates that the hybridizations between anions and irons, i.e., the amplitudes of the hopping parameters also widely vary. In contrast, in cuprates, the distance between Cu and O in the CuO<sub>2</sub> plane does not largely depend on compounds. Thus, the amplitude of the hopping parameters does not largely change in cuprates. This difference in the lattice structures induces the different parameter dependence of  $T_c$ . Nevertheless, we note that the normalized electron correlation  $U/t$  plays some role in stabilizing high- $T_c$  superconductivity since  $U/t$  changes in both iron-based superconductors and cuprates.

For performing the PCA, we employ 36 microscopic parameters as the descriptors, which consist of the Coulomb interactions ( $V_{ij}$ ), the Hund couplings ( $J_{ij}$ ), and the hopping parameters ( $t_{ij}$ ). We obtain  $\lambda_1 = 25.06$ ,  $\lambda_2 = 7.94$ ,  $\lambda_3 = 2.12$ ,  $\lambda_4 = 1.20$ , and  $\lambda_5 = 0.37$  as the five dominant principal values. The first and the second principal values are large compared with the other principal values, and hence it is expected that the first and the second principal vectors ( $\mathbf{v}^1$  and  $\mathbf{v}^2$ ) accurately reflect the material dependence. In Fig. 4(a), we plot the absolute value of each component comprising these vectors. We find that the interaction parameters (such as onsite and offsite Coulomb interactions) govern the first principal vector while the hopping parameters and Hund couplings govern the second principal vector.

We plot the first and the second principal components ( $y_1^{(n)}$  and  $y_2^{(n)}$ ) in Fig. 4(b). For 1111 and 111 compounds, we find that the second component characterizes the differences within families, i.e., the same family has a similar first component, but each compound in the family has a different second component. For example, the first component of the 1111 family is approximately four, but the second component varies from -3.2 to 6.0. In contrast, we find that 122 and 42622 compounds exhibit opposite tendencies: the same family has a similar second component, but each compound has a different first component. We note that the first component changes significantly by changing the total electron density for 1111 and 122 families.

The 11 family exhibits exceptional behavior, i.e., both the first and the second components exhibit considerable compound dependence. This exceptional behavior may be related to exotic phenomena such as the absence of antiferromagnetic order and the high- $T_c$  superconductivity in a monolayer occurring in FeSe [107–109].

In Fig. 4(c) and (d), we plot  $T_c$  as a function of the first and the second principal components. We find that  $T_c$  is better correlated with the second component than the first component. In particular, we find that the dependence of  $T_c$  on the second component is manifested as a dome structure reminiscent of Lee’s plot [78, 79]. This result indicates that the difference in the microscopic parameters associated with the effective Hamiltonians provides sufficient information for explaining the compound dependence of  $T_c$ . By constructing the regression model for reproducing  $T_c$ , we show that these parameters allow quantitative reproduction of this dependence.

## 2. Regression model for estimating $T_c$

After determining the best regression model within the nested CV approach explained in Sec. II, we obtain our predictor using all the  $T_c$  data obtained in the experiments. Figure 5(a) shows the accuracy of the obtained regression model. We find that this model reproduces the experimental  $T_c$  data, as indicated by the high coefficient of determination ( $R^2 \approx 0.92$ ). This result confirms that

our regression model can predict the  $T_c$  of associated with several different families for iron-based superconductors.

We apply our predictor to low-energy Hamiltonians for a hypothetical compound, whose lattice structure is systematically changed from that of LaFeAsO. We vary the fractional coordinates of two As atoms as  $(0.5, 0.0, \gamma f_{\text{As}})$  and  $(0.0, 0.5, 1-\gamma f_{\text{As}})$ ;  $f_{\text{As}}$  is the fractional coordinate of As for the original LaFeAsO, namely  $f_{\text{As}} = 0.6512$  [2], and the parameter  $\gamma$  indicates changes in the height of As from the Fe plane. A schematic showing this lattice distortion is presented in the inset of Fig. 5(b). Note that the fractional coordinates of the other atoms and the lattice constants do not change.

We obtain the low-energy effective Hamiltonians for the hypothetical compounds. From the microscopic parameters in the Hamiltonians, we calculate the  $T_c$  of each compound using the regression model. In Fig. 5(b), we show the  $\gamma$  dependence of  $T_c$  for hypothetical LaFeAsO materials. We find that  $T_c$  increases with increasing  $\gamma$  and vice versa. At  $\gamma \sim 1.03$ ,  $T_c$  reaches  $\sim 100\text{K}$ . The applicability range of the regression model is limited to the parameter space around the existing compounds, and therefore the role of lattice distortion in inducing high- $T_c$  superconductivity ( $T_c \approx 100\text{K}$ ) remains unclear. Nevertheless, the qualitative behavior of  $T_c$  may be correctly predicted by the regression model. This result indicates that our regression model captures the essence of Lee’s plot [78, 79] and the theoretical study [24], which suggests that the height of As from the Fe plane plays a key role in determining the compound dependence of  $T_c$ .

Here, we examine the relation between enhancement of  $T_c$  and the microscopic parameters. As shown in Fig. 6(a), the maximum value of the nearest hoppings  $t_{\text{max}}$  decreases by increasing  $\gamma$  while  $\bar{U}$  has a broad peak around  $\gamma \sim 1.04$ . This result indicates that we can enhance  $T_c$  of LaFeAsO by increasing the amplitude of the electronic correlations. In Fig. 6(b), we plot the first and the second principal components for the virtual materials. We find that the changes in the second principal component governs the enhancement of  $T_c$  around LaFeAsO. This plot also indicates that LaFeAsO is located at the edge of the existing materials in the  $y_1 - y_2$  plane. Therefore, it is plausible that we can reach the unexplored region and enhance  $T_c$  by changing the height of As in LaFeAsO.

We also consider the possibility of realizing hypothetical materials. In our *ab initio* calculations of such materials, we do not perform the structure optimization and simulations for phonon’s properties. Therefore, our proposed materials may be unattainable for the conventional bulk system at ambient pressure. Stable materials may be used to obtain an interface structure. Such interface or thin-film structures induce drastic changes in the electronic states of target materials and may enhance  $T_c$ . Successful experiments applying this approach have already been reported for high- $T_c$  superconductors such as  $\text{La}_2\text{CuO}_4$  and FeSe [109, 110]. The material structure can also be controlled via laser irradiation, which has been

successfully applied to FeSe[111]. In that work, strong laser irradiation led to changes in the height of Se atoms from the Fe-Fe plane. This results from the dispersive excitation of coherent phonon mechanism[112], which governs the excitation of  $A_{1g}$  Raman active modes. These modes also occur in LaFeAsO[113], and hence we expect that our predicted structure would be realized via laser irradiation.

#### IV. SUMMARY

In summary, we have derived the low-energy effective Hamiltonians for 32 iron-based compounds and four related compounds using the *ab initio* downfolding method. We have found that microscopic parameters such as the hopping parameters and the Coulomb interaction are associated with a wide range of iron-based superconductors. To systematically characterize the compound dependence of the microscopic parameters, we perform the PCA. As a result, we find that the first principal vector consists of mainly interaction terms, while the second consists of mainly hopping terms. We show that the first principal values characterize the difference within the 42622 and 122 families while the second principal values characterize the difference within the 1111 and 111 families. Moreover, we show that the compound dependence of  $T_c$  with respect to the second principal value is manifested as a dome structure reminiscent of Lee's plot [78, 79]. This result suggests that the obtained microscopic parameters adequately reflect the compound dependence of  $T_c$ .

Afterward, we construct a regression model for reproducing the compound dependence of  $T_c$  from the microscopic parameters of the *ab initio* Hamiltonians. We succeed in reproducing experimental  $T_c$  values of the iron-based superconductors ( $R^2 \approx 0.92$ ). Using the regression model, we show that the  $T_c$  of LaFeAsO can be enhanced by properly changing the As height from the Fe plane. Such a hypothetical structure would be realized in experiments including laser irradiation processes. Applying pressure can also control the anion height from the Fe plane, and this is accompanied by changes in the lattice constants[115–117]. It has been reported that  $T_c$  increases to about 50 K by applying pressure into LaFeAsO[117]. However, the current regression model does not have enough accuracy to quantitatively reproduce the experiments because the dataset does not include the experimental data under pressure. Future studies will determine whether our approach can reproduce  $T_c$  of iron-based superconductors under pressure by updating the dataset. Using cutting-edge numerical packages (such as mVMC[118]) to directly solve the low-energy effective Hamiltonians in order to determine whether  $T_c$  is really enhanced for the hypothetical structures would be an intriguing challenge. However, the numerical cost of such calculations is rather high and hence this analysis will be considered in future studies.

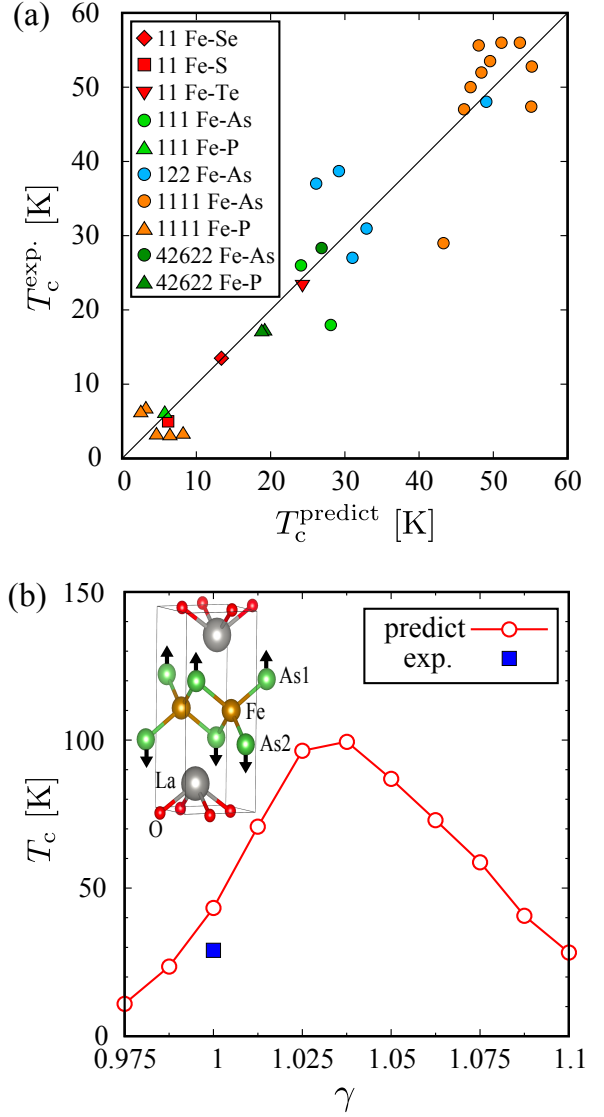


FIG. 5. (color online) (a) Experimental  $T_c$  vs. predicted  $T_c$  obtained from our regression model. Notations are the same as those of Fig. 2. The black thin line represents  $T_c^{\text{predict}} = T_c^{\text{exp.}}$ . The coefficient determination  $R^2$  is about 0.92. Data is also shown in Table II. Note that  $\text{SrFe}_2\text{As}_{1.3}\text{P}_{0.7}$  and  $\text{BaFe}_2\text{As}_{1.48}\text{P}_{0.52}$  are categorized as Fe – As, and  $\text{FeSe}_{0.4}\text{Te}_{0.6}$  is categorized as Fe – Te. (b) Prediction of  $T_c$  for LaFeAsO with hypothetical structures with different c-axis components of fractional coordinates corresponding to As,  $f_{\text{As}}$ .  $\gamma$  corresponds to the ratio of  $f_{\text{As}}$  associated with the original LaFeAsO[2] to that of the hypothetical materials. Note that only the material for  $\gamma = 1$  has been found in the experiments; the corresponding  $T_c$  is plotted as the blue square. Inset represents the structure of the original LaFeAsO, which is depicted using VESTA[114]. The fractional coordinates of two As atoms, As1 and As2, are set to  $(0.5, 0.0, \gamma f_{\text{As}})$  and  $(0.0, 0.5, 1 - \gamma f_{\text{As}})$ , respectively. Black thick arrows denote the displacement pattern of the Raman-active  $A_{1g}$  phonon.

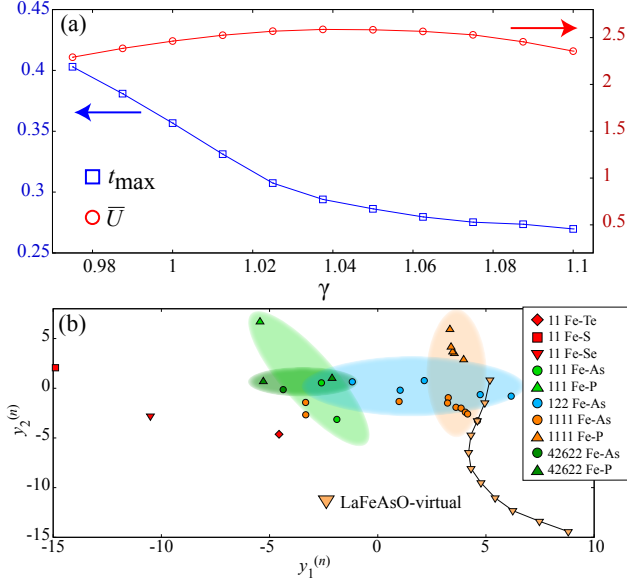


FIG. 6. (color online) (a)  $\gamma$  dependence of  $\bar{U}$  and  $t_{\max}$  for the virtual compounds. The units of  $\bar{U}$  and  $t_{\max}$  are eV. (b) The first and second principal components for the virtual compounds. The definition of the principal component is given in Eq. (11). The other points are the same as in Fig. 4(b).

The present work shows the possibility that the data-science techniques can help us to bypass a difficult problem –*solving the Hamiltonians for quantum many-body systems*– and to clarify the effect of microscopic parameters on superconductivity. Further applications of the developed method to other exotic phenomena (such as the correlated topological materials) may be considered in future work.

*Acknowledgments.*— We acknowledge Tetsuya Shoji, Noritsugu Sakuma, Mitsuaki Kawamura, Takashi Miyake and Kazuma Nakamura for fruitful discussions and important suggestions. We also thank Mitsuaki Kawamura for providing us his scripts to generate inputs for Quantum ESPRESSO and RESPACK. Some of the calculations were performed by using the Supercomputer Center, located at the Institute for Solid State Physics, the University of Tokyo. A part of this work is financially supported by TOYOTA MOTOR CORPORATION. The authors were supported by Building of Consortia for the Development of Human Resources in Science and Technology from the MEXT of Japan. This work has been also supported by a Grant-in-Aid for Scientific Research (Nos. 16H06345 and 20H01850) from Ministry of Education, Culture, Sports, Science and Technology, Japan.

## Appendix A: Features of Descriptors

Here, we summarize the features of the descriptors used in constructing the regression models and the PCA. In constructing the regression models, we prepare 72 models based on the seven choices shown in Table III.

In addition, all the models include  $t_{p,\text{all}}$  ( $p=\text{mean,max}$ ) and  $U_{p,\text{diag}}$  ( $p=\text{mean,max,min}$ ). We standardized these descriptors for the construction of the regression model. In Table IV, we list the descriptors used in PCA in descending order of the absolute value corresponding to the components of the first principal vector,  $|v_i^1|$ .

## Appendix B: Construction of regression model with undersampling

In this appendix, we discuss the effect of undersampling on our database. Our database listed in Table II

contains 29 materials, but almost half of them are labeled as 1111 compounds. Such an imbalance in the dataset sometime causes overfitting problems in constructing the regression model.

To check whether the overfitting happens or not, we construct the regression model using the database with undersampling, which means that we remove several 1111 compounds from the training data. Figure 7(a) shows the accuracy of our regression model with the undersampling. We find that the model with the undersampling also reproduces the experimental  $T_c$  data with  $R^2 \approx 0.90$ . The predicted  $T_c$  for 1111 compounds treated as the test data well reproduce the experimental ones. This model also predicts almost the same results for  $T_c$  for LaFeAsO with a hypothetical structure, shown in Fig. 7 (b). This result suggests that the overfitting does not occur in the predicted results in the main text, and thus, the original dataset without the undersampling is reasonable.

- 
- [1] B. Keimer, S. A. Kivelson, M. R. Norman, S. Uchida, and J. Zaanen: *Nature* **518** (2015) 179.
  - [2] Y. Kamihara, T. Watanabe, M. Hirano, and H. Hosono: *J. Am. Chem. Soc.* **130** (2008) 3296.
  - [3] G. R. Stewart: *Rev. Mod. Phys.* **83** (2011) 1589.
  - [4] H. Hosono and K. Kuroki: *Physica C: Superconductivity and its Applications* **514** (2015) 399.
  - [5] Q. Si, R. Yu, and E. Abrahams: *Nat. Rev. Mater.* **1** (2016) 16017.
  - [6] M. Imada and T. Miyake: *J. Phys. Soc. Jpn.* **79** (2010) 112001.
  - [7] F. Aryasetiawan, M. Imada, A. Georges, G. Kotliar, S. Biermann, and A. I. Lichtenstein: *Phys. Rev. B* **70** (2004) 195104.
  - [8] T. Misawa and M. Imada: *Nat. Commun.* **5** (2014) 5738.
  - [9] T. Ohgoe, M. Hirayama, T. Misawa, K. Ido, Y. Yamaji, and M. Imada: *Phys. Rev. B* **101** (2020) 045124.
  - [10] L. Himanen, A. Geurts, A. S. Foster, and P. Rinke: *Adv. Sci.* **6** (2019) 1900808.
  - [11] M. Klintenberg and O. Eriksson: *Comput. Mater. Sci.* **67** (2013) 282.
  - [12] O. Isayev, D. Fourches, E. N. Muratov, C. Oses, K. Rasch, A. Tropsha, and S. Curtarolo: *Chem. Mater.* **27** (2015) 735.
  - [13] T. O. Owolabi, K. O. Akande, and S. O. Olatunji: *J. Supercond. Nov. Magn.* **28** (2015) 75.
  - [14] V. Stanev, C. Oses, A. G. Kusne, E. Rodriguez, J. Paglione, S. Curtarolo, and I. Takeuchi: *npj Comput. Mater.* **4** (2018) 29.
  - [15] K. Matsumoto and T. Horide: *Appl. Phys. Express* **12** (2019) 073003.
  - [16] T. Konno, H. Kurokawa, F. Nabeshima, Y. Sakishita, R. Ogawa, I. Hosako, and A. Maeda: *Phys. Rev. B* **103** (2021) 014509.
  - [17] B. Roter and S. Dordevic: *Physica C* **575** (2020) 1353689.
  - [18] Z.-L. Liu, P. Kang, Y. Zhu, L. Liu, and H. Guo: *APL Mater.* **8** (2020) 061104.
  - [19] O. Akomolafe, T. O. Owolabi, M. A. Abd Rahman, M. M. Awang Kechik, M. N. M. Yasin, and M. Souiyah: *Materials* **14** (2021) 4604.
  - [20] D. J. Singh and M.-H. Du: *Phys. Rev. Lett.* **100** (2008) 237003.
  - [21] Z. P. Yin, S. Lebegue, M. J. Han, B. P. Neal, S. Y. Savrasov, and W. E. Pickett: *Phys. Rev. Lett.* **101** (2008) 047001.
  - [22] K. Kuroki, S. Onari, R. Arita, H. Usui, Y. Tanaka, H. Kontani, and H. Aoki: *Phys. Rev. Lett.* **101** (2008) 087004.
  - [23] I. I. Mazin, D. J. Singh, M. D. Johannes, and M. H. Du: *Phys. Rev. Lett.* **101** (2008) 057003.
  - [24] K. Kuroki, H. Usui, S. Onari, R. Arita, and H. Aoki: *Phys. Rev. B* **79** (2009) 224511.
  - [25] T. Miyake, K. Nakamura, R. Arita, and M. Imada: *J. Phys. Soc. Jpn.* **79** (2010) 044705.
  - [26] P. Giannozzi, O. Andreussi, T. Brumme, O. Bunau, M. B. Nardelli, M. Calandra, R. Car, C. Cavazzoni, D. Ceresoli, M. Cococcioni, et al.: *J. Phys. Condens. Matter* **29** (2017) 465901.
  - [27] M. Schlipf and F. Gygi: *Comput. Phys. Commun.* **196** (2015) 36.
  - [28] D. R. Hamann: *Phys. Rev. B* **88** (2013) 085117.
  - [29] S. W. Jang, H. Sakakibara, H. Kino, T. Kotani, K. Kuroki, and M. J. Han: *Sci. Rep.* **6** (2016) 33397.
  - [30] M. Kawamura, Y. Gohda, and S. Tsuneyuki: *Phys. Rev. B* **89** (2014) 094515.
  - [31] K. Nakamura, Y. Yoshimoto, Y. Nomura, T. Tadano, M. Kawamura, T. Kosugi, K. Yoshimi, T. Misawa, and Y. Motoyama: *Comput. Phys. Commun.* **261** (2021) 107781.
  - [32] N. Marzari and D. Vanderbilt: *Phys. Rev. B* **56** (1997) 12847.
  - [33] I. Souza, N. Marzari, and D. Vanderbilt: *Phys. Rev. B* **65** (2001) 035109.
  - [34] M. Aichhorn, S. Biermann, T. Miyake, A. Georges, and M. Imada: *Phys. Rev. B* **82** (2010) 064504.

TABLE III. Choices of descriptors used in the regression model. Our choices when constructing the best regression model are shown in the second column.

Choices of Descriptors	Best model
Normalizing all the descriptors except for $t_{\max, \text{all}}$ by $t_{\max, \text{all}}$	True
Using square of descriptors (e.g., $U_{\text{mean,diag}}^2$ )	True
Using cross terms (e.g., $U_{\text{mean,diag}} \times t_{\max, \text{all}}$ )	True
Including $V_{\max, \text{diag}}$ , $V_{\min, \text{diag}}$ , $V_{\text{mean,diag}}$	False
Including $J_{\max, \text{offdiag}}$ , $J_{\min, \text{offdiag}}$ , $J_{\text{mean,offdiag}}$	False
Including $V_{\text{mean,diag}}/U_{\max, \text{diag}}$ when $V_{\text{mean,diag}}$ is used as the descriptor	–
Including $J_{\text{mean,offdiag}}/U_{\max, \text{diag}}$ when $J_{\text{mean,offdiag}}$ is used as the descriptor	–

- [35] M. Hirayama, T. Misawa, T. Ohgoe, Y. Yamaji, and M. Imada: Phys. Rev. B **99** (2019) 245155.
- [36] F. Nilsson, K. Karlsson, and F. Aryasetiawan: Phys. Rev. B **99** (2019) 075135.
- [37] T. Miyake, F. Aryasetiawan, and M. Imada: Phys. Rev. B **80** (2009) 155134.
- [38] E. Şaşıoğlu, C. Friedrich, and S. Blügel: Phys. Rev. B **83** (2011) 121101(R).
- [39] H. Usui and K. Kuroki: Phys. Rev. Res. **1** (2019) 033025.
- [40] K. Rajan, C. Suh, and P. F. Mendez: Stat. Anal. Data Min. **1** (2009) 361.
- [41] C. M. Bishop: *Pattern Recognition and Machine Learning* (Springer, 2006).
- [42] M. Stone: J. R. Stat. Soc. **36** (1974) 111.
- [43] R. Tibshirani: J. R. Stat. Soc. **58** (1996) 267.
- [44] F. Pedregosa, G. Varoquaux, A. Gramfort, V. Michel, B. Thirion, O. Grisel, M. Blondel, P. Prettenhofer, R. Weiss, V. Dubourg, J. Vanderplas, A. Passos, D. Cournapeau, M. Brucher, M. Perrot, and E. Duchesnay: J. Mach. Learn. Res. **12** (2011) 2825.
- [45] T. Akiba, S. Sano, T. Yanase, T. Ohta, and M. Koyama: Proceedings of the 25th ACM SIGKDD International Conference on Knowledge Discovery and Data Mining, KDD '19, 2019, pp. 2623–2631.
- [46] G. Bergerhoff, R. Hundt, R. Sievers, and I. Brown: J. Chem. Inf. Comput. Sci. **23** (1983) 66.
- [47] D. Zagorac, H. Müller, S. Ruehl, J. Zagorac, and S. Rehme: J. Appl. Crystallogr. **52** (2019) 918.
- [48] <https://materials.springer.com/>.
- [49] T. Miyake, T. Kosugi, S. Ishibashi, and K. Terakura: J. Phys. Soc. Jpn. **79** (2010) 123713.
- [50] X. Lai, H. Zhang, Y. Wang, X. Wang, X. Zhang, J. Lin, and F. Huang: J. Am. Chem. Soc. **137** (2015) 10148.
- [51] M. Lehman, A. Llobet, K. Horigane, and D. Louca: J. Phys. Conf. Ser. **251** (2010) 012009.
- [52] V. Awana, A. Pal, A. Vajpayee, B. Gahtori, and H. Kishan: Physica C **471** (2011) 77.
- [53] T. Hanna, Y. Muraba, S. Matsuishi, N. Igawa, K. Kodama, S.-i. Shamoto, and H. Hosono: Phys. Rev. B **84** (2011) 024521.
- [54] Y. Xiao, Y. Su, R. Mittal, T. Chatterji, T. Hansen, S. Price, C. Kumar, J. Persson, S. Matsuishi, Y. Inoue, et al.: Phys. Rev. B **81** (2010) 094523.
- [55] S. Matsuishi, Y. Inoue, T. Nomura, H. Yanagi, M. Hirano, and H. Hosono: J. Am. Chem. Soc. **130** (2008) 14428.
- [56] Y. Kamihara, H. Hiramatsu, M. Hirano, R. Kawamura, H. Yanagi, T. Kamiya, and H. Hosono: J. Am. Chem. Soc. **128** (2006) 10012.
- [57] B. I. Zimmer, W. Jeitschko, J. H. Albering, R. Glaum, and M. Reehuis: J. Alloys Compd. **229** (1995) 238.
- [58] J. Zhao, Q. Huang, C. de la Cruz, S. Li, J. W. Lynn, Y. Chen, M. A. Green, G. F. Chen, G. Li, Z. Li, J. L. Luo, N. L. Wang, and P. Dai: Nat. Mater. **7** (2008) 953.
- [59] F. Nitsche, A. Jesche, E. Hieckmann, T. Doert, and M. Ruck: Phys. Rev. B **82** (2010) 134514.
- [60] F. Nitsche, T. Doert, and M. Ruck: Solid State Sci. **19** (2013) 162.
- [61] Z. Deng, X. Wang, Q. Liu, S. Zhang, Y. Lv, J. Zhu, R. Yu, and C. Jin: EPL **87** (2009) 37004.
- [62] I. Morozov, A. Boltalin, O. Volkova, A. Vasiliev, O. Kataeva, U. Stockert, M. Abdel-Hafiez, D. Bombor, A. Bachmann, L. Harnagea, et al.: Cryst. Growth Des. **10** (2010) 4428.
- [63] D. R. Parker, M. J. Pitcher, P. J. Baker, I. Franke, T. Lancaster, S. J. Blundell, and S. J. Clarke: Chem. Commun. (2009) 2189.
- [64] P. Wenz and H.-U. Schuster: Z. Naturforsch. B **39** (1984) 1816.
- [65] KFe2P2 Crystal Structure: Datasheet from “PAULING FILE Multinaries Edition – 2012” in SpringerMaterials (<https://materials.springer.com/isp/crystallographic/docs/sd.2110357>).
- [66] M. Reehuis and W. Jeitschko: J. Phys. Chem. Solids. **51** (1990) 961.
- [67] S. R. Saha, K. Kirshenbaum, N. P. Butch, J. Paglione, and P. Zavalij: J. Phys. Conf. Ser. **273** (2011) 012104.
- [68] M. Rotter, C. Hieke, and D. Johrendt: Phys. Rev. B **82** (2010) 014513.
- [69] S. Rózsa and H.-U. Schuster: Z. Naturforsch. B **36** (1981) 1668.
- [70] B. Sagarov, C. Cantoni, M. Pan, T. C. Hogan, W. Ratcliff II, S. D. Wilson, K. Fritsch, M. Tachibana, B. D. Gaulin, and A. S. Sefat: Sci. Rep. **4** (2014) 4120.
- [71] F. Rullier-Albenque, D. Colson, A. Forget, P. Thuéry, and S. Poissonnet: Phys. Rev. B **81** (2010) 224503.
- [72] H. Ogino, Y. Matsumura, Y. Katsura, K. Ushiyama, S. Horii, K. Kishio, and J.-i. Shimoyama: Supercond. Sci. Technol. **22** (2009) 075008.
- [73] P. M. Shirage, K. Kihou, C.-H. Lee, H. Kito, H. Eisaki, and A. Iyo: Appl. Phys. Lett. **97** (2010) 172506.
- [74] B. Sagarov, D. J. Singh, V. O. Garlea, and A. S. Sefat: Sci. Rep. **3** (2013) 2154.
- [75] E. Brechtel, G. Cordier, and H. Schäfer: Z. Naturforsch. B **33** (1978) 820 .

TABLE IV. Descriptors used in PCA

$i$	descriptor
0	$V_{\min, \text{diag}}$
1	$V_{\min, \text{offdiag}}$
2	$V_{\text{mean}, \text{diag}}$
3	$V_{\text{mean}, \text{all}}$
4	$V_{\text{mean}, \text{offdiag}}$
5	$V_{\text{max}, \text{offdiag}}$
6	$V_{\text{max}, \text{diag}}$
7	$V'_{\min, \text{diag}}$
8	$V'_{\min, \text{offdiag}}$
9	$V'_{\text{mean}, \text{diag}}$
10	$V'_{\text{mean}, \text{all}}$
11	$V'_{\text{mean}, \text{offdiag}}$
12	$V'_{\text{max}, \text{offdiag}}$
13	$V'_{\text{max}, \text{diag}}$
14	$U_{\min, \text{offdiag}}$
15	$U_{\text{mean}, \text{offdiag}}$
16	$U_{\text{max}, \text{offdiag}}$
17	$U_{\text{mean}, \text{all}}$
18	$U_{\text{mean}, \text{diag}}$
19	$U_{\text{max}, \text{diag}}$
20	$U_{\min, \text{diag}}$
21	$J_{\text{mean}, \text{offdiag}}$
22	$J_{\text{max}, \text{offdiag}}$
23	$t_{\text{mean}, \text{offdiag}}$
24	$t_{\text{max}, \text{diag}}$
25	$J_{\min, \text{offdiag}}$
26	$t_{\min, \text{diag}}$
27	$t_{\text{mean}, \text{all}}$
28	$t'_{\min, \text{diag}}$
29	$t'_{\text{max}, \text{offdiag}}$
30	$t'_{\text{mean}, \text{offdiag}}$
31	$t_{\text{mean}, \text{diag}}$
32	$t_{\text{max}, \text{offdiag}}$
33	$t'_{\text{max}, \text{diag}}$
34	$t'_{\text{mean}, \text{all}}$
35	$t'_{\text{mean}, \text{diag}}$

- [76] A. S. Sefat, M. A. McGuire, R. Jin, B. C. Sales, D. Mandrus, F. Ronning, E. D. Bauer, and Y. Mozharivskyj: Phys. Rev. B **79** (2009) 094508.
- [77] T. Watanabe, H. Yanagi, Y. Kamihara, T. Kamiya, M. Hirano, and H. Hosono: J. Solid State Chem. **181** (2008) 2117.
- [78] C.-H. Lee, A. Iyo, H. Eisaki, H. Kito, M. Teresa Fernandez-Diaz, T. Ito, K. Kihou, H. Matsuhata, M. Braden, and K. Yamada: J. Phys. Soc. Jpn. **77** (2008) 083704.
- [79] Y. Mizuguchi and Y. Takano: J. Phys. Soc. Jpn. **79** (2010) 102001.
- [80] Y. Mizuguchi, F. Tomioka, S. Tsuda, T. Yamaguchi,

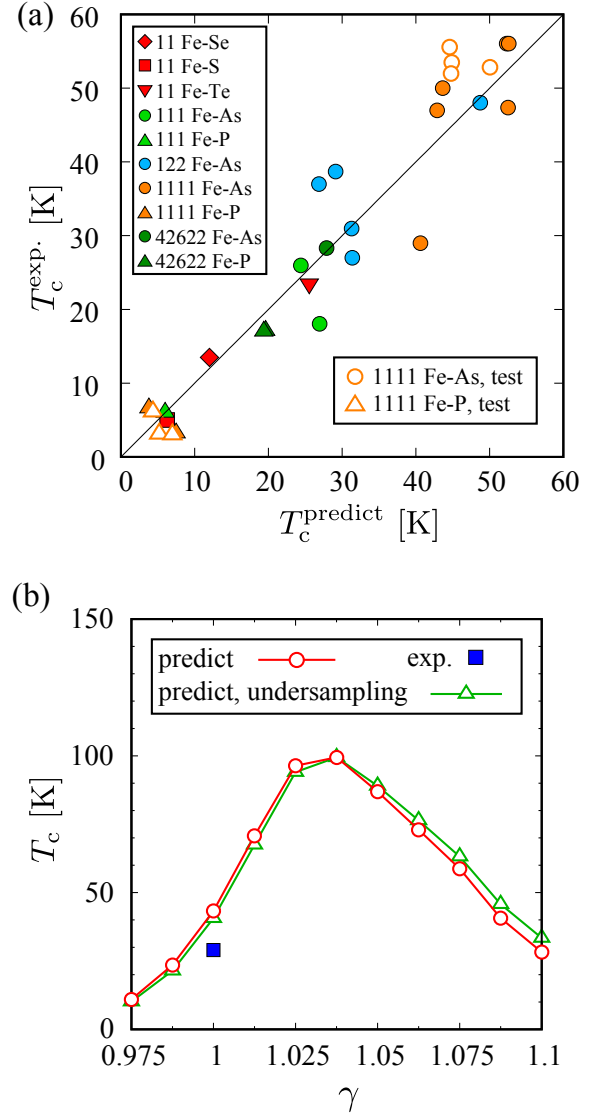


FIG. 7. (color online) (a) Experimental  $T_c$  vs. predicted  $T_c$  obtained from the regression model with the undersampling, which removes four 1111-As compounds (GdFeAsO, NdFeAsO, SmFeAsO, PrFeAsO) and three 1111-P compounds (GdFePO, NdFePO, SmFePO) from the training data. Open symbols mean the results for 1111 compounds treated as the test data. The other notations are the same as those of Fig. 5. The coefficient determination  $R^2$  is about 0.90. (b)  $T_c$  for LaFeAsO with hypothetical structures predicted by the regression model. Red circles and blue squares are the same results plotted in Fig. 5. Green triangles represent the  $T_c$  of LaFeAsO with hypothetical structures predicted by using the model with the undersampling.

- and Y. Takano: Appl. Phys. Lett. **93** (2008) 152505.
- [81]  $T_c^{\text{exp.}}$  is estimated from a figure where the temperature dependence of the electronic specific heat is shown.
- [82] T. Noji, M. Imaizumi, T. Suzuki, T. Adachi, M. Kato, and Y. Koike: J. Phys. Soc. Jpn. **81** (2012) 054708.

- [83] Y. Muraba, S. Matsuishi, and H. Hosono: J. Phys. Soc. Jpn. **83** (2014) 033705.
- [84] G. Wu, Y. L. Xie, H. Chen, M. Zhong, R. H. Liu, B. C. Shi, Q. J. Li, X. F. Wang, T. Wu, Y. J. Yan, J. J. Ying, and X. H. Chen: J. Phys. Condens. Matter **21** (2009) 142203.
- [85] P. Cheng, B. Shen, G. Mu, X. Zhu, F. Han, B. Zeng, and H.-H. Wen: EPL **85** (2009) 67003.
- [86] R. E. Baumbach, J. J. Hamlin, L. Shu, D. A. Zocco, N. M. Crisosto, and M. B. Maple: New J. Phys. **11** (2009) 025018.
- [87] Y. Kamihara, H. Hiramatsu, M. Hirano, Y. Kobayashi, S. Kitao, S. Higashitaniguchi, Y. Yoda, M. Seto, and H. Hosono: Phys. Rev. B **78** (2008) 184512.
- [88] C. Liang, R. Che, F. Xia, X. Zhang, H. Cao, and Q. Wu: J. Alloys Compd. **507** (2010) 93.
- [89] LaFeAsO<sub>1-x</sub>H<sub>x</sub> has the two-dome  $T_c$  structure.  $T_c^{\text{exp}}$  is used the maximum  $T_c$  of the dome in the low-doping region.
- [90] S. Iimura, S. Matsuishi, H. Sato, T. Hanna, Y. Muraba, S. W. Kim, J. E. Kim, M. Takata, and H. Hosono: Nat. Commun. **3** (2012) 943.
- [91] S. Matsuishi, T. Hanna, Y. Muraba, S. W. Kim, J. E. Kim, M. Takata, S.-i. Shamoto, R. I. Smith, and H. Hosono: Phys. Rev. B **85** (2012) 014514.
- [92] Z. A. Ren, J. Yang, W. Lu, W. Yi, G. C. Che, X. L. Dong, L. L. Sun, and Z. X. Zhao: Mater. Res. Innov. **12** (2008) 105.
- [93] A. Adamski, C. Krellner, and M. Abdel-Hafiez: Phys. Rev. B **96** (2017) 100503(R).
- [94] Y. Kamihara, T. Nomura, M. Hirano, J. Eun Kim, K. Kato, M. Takata, Y. Kobayashi, S. Kitao, S. Higashitaniguchi, Y. Yoda, M. Seto, and H. Hosono: New J. Phys. **12** (2010) 033005.
- [95] J. Yang, Z.-C. Li, W. Lu, W. Yi, X.-L. Shen, Z.-A. Ren, G.-C. Che, X.-L. Dong, L.-L. Sun, F. Zhou, and Z.-X. Zhao: Supercond. Sci. Technol. **21** (2008) 082001.
- [96] K. A. Yates, K. Morrison, J. A. Rodgers, G. B. S. Penny, J.-W. G. Bos, J. P. Attfield, and L. F. Cohen: New J. Phys. **11** (2009) 025015.
- [97] X.-c. Wang, Q.-q. Liu, L.-x. Yang, Z. Deng, Y.-x. Lü, W.-b. Gao, S.-j. Zhang, R.-c. Yu, and C.-q. Jin: Front. Phys. China **4** (2009) 464.
- [98] X. Wang, Q. Liu, Y. Lv, W. Gao, L. Yang, R. Yu, F. Li, and C. Jin: Solid State Commun. **148** (2008) 538.
- [99] H. L. Shi, H. X. Yang, H. F. Tian, J. B. Lu, Z. W. Wang, Y. B. Qin, Y. J. Song, and J. Q. Li: J. Phys. Condens. Matter **22** (2010) 125702.
- [100] S. Kasahara, T. Shibauchi, K. Hashimoto, K. Ikada, S. Tonegawa, R. Okazaki, H. Shishido, H. Ikeda, H. Takeya, K. Hirata, T. Terashima, and Y. Matsuda: Phys. Rev. B **81** (2010) 184519.
- [101] K. Sasmal, B. Lv, B. Lorenz, A. M. Guloy, F. Chen, Y.-Y. Xue, and C.-W. Chu: Phys. Rev. Lett. **101** (2008) 107007.
- [102] It is not fully clarified whether the system shows the bulk superconductivity.
- [103] K. Kudo, K. Iba, M. Takasuga, Y. Kitahama, J.-i. Matsumura, M. Danura, Y. Nogami, and M. Nohara: Sci. Rep. **3** (2013) 1478.
- [104] M. Rotter, M. Tegel, and D. Johrendt: Phys. Rev. Lett. **101** (2008) 107006.
- [105] J.-B. Morée, M. Hirayama, M. T. Schmid, Y. Yamaji, and M. Imada: Phys. Rev. B **106** (2022) 235150.
- [106] M. Hirayama, M. T. Schmid, T. Tadano, T. Misawa, and M. Imada: arXiv (2022).
- [107] F.-C. Hsu, J.-Y. Luo, K.-W. Yeh, T.-K. Chen, T.-W. Huang, P. M. Wu, Y.-C. Lee, Y.-L. Huang, Y.-Y. Chu, D.-C. Yan, et al.: Proc. Natl. Acad. Sci. U.S.A. **105** (2008) 14262.
- [108] S. Li, C. de La Cruz, Q. Huang, Y. Chen, J. Lynn, J. Hu, Y.-L. Huang, F.-C. Hsu, K.-W. Yeh, M.-K. Wu, et al.: Phys. Rev. B **79** (2009) 054503.
- [109] W. Qing-Yan, L. Zhi, Z. Wen-Hao, Z. Zuo-Cheng, Z. Jin-Song, L. Wei, D. Hao, O. Yun-Bo, D. Peng, C. Kai, et al.: Chin. Phys. Lett. **29** (2012) 037402.
- [110] J. Wu, O. Pelleg, G. Logvenov, A. Bollinger, Y. Sun, G. Boebinger, M. Vanević, Z. Radović, and I. Božović: Nat. Mater. **12** (2013) 877.
- [111] T. Suzuki, T. Someya, T. Hashimoto, S. Michimae, M. Watanabe, M. Fujisawa, T. Kanai, N. Ishii, J. Itatani, S. Kasahara, et al.: Commun. Phys. **2** (2019) 115.
- [112] H. J. Zeiger, J. Vidal, T. K. Cheng, E. P. Ippen, G. Dresselhaus, and M. S. Dresselhaus: Phys. Rev. B **45** (1992) 768.
- [113] V. G. Hadjiev, M. N. Iliev, K. Sasmal, Y.-Y. Sun, and C. W. Chu: Phys. Rev. B **77** (2008) 220505(R).
- [114] K. Momma and F. Izumi: J. Appl. Crystallogr. **44** (2011) 1272.
- [115] H. Okada, K. Igawa, H. Takahashi, Y. Kamihara, M. Hirano, H. Hosono, K. Matsubayashi, and Y. Uwatoko: J. Phys. Soc. Jpn. **77** (2008) 113712.
- [116] H. Okabe, N. Takeshita, K. Horigane, T. Muranaka, and J. Akimitsu: Phys. Rev. B **81** (2010) 205119.
- [117] K. Kobayashi, J.-i. Yamaura, S. Iimura, S. Maki, H. Sagayama, R. Kumai, Y. Murakami, H. Takahashi, S. Matsuishi, and H. Hosono: Sci. Rep. **6** (2016) 39646.
- [118] T. Misawa, S. Morita, K. Yoshimi, M. Kawamura, Y. Motoyama, K. Ido, T. Ohgoe, M. Imada, and T. Kato: Comput. Phys. Commun. **235** (2019) 447.